Biomedical Physics & Engineering Express

PAPER

Relating diffusion-weighted magnetic resonance imaging of brain white matter to cognitive processing-speed deficits in schizophrenia

Muhammad Anisuzzaman Talukder
Department of Electrical and Electronic Engineering, Bangladesh University of Engineering and Technology, Dhaka 1205, Bangladesh
E-mail: anis@eee.buet.ac.bd

RECEIVED
24 February 2020
REVISED
3 July 2020
ACCEPTED FOR PUBLICATION
7 July 2020
PUBLISHED
15 July 2020

Keywords: magnetic resonance imaging, diffusional kurtosis imaging, brain white matter, cognitive processing speed

Abstract

Diffusion tensor imaging (DTI) and diffusion kurtosis imaging (DKI) analyses of diffusion-weighted magnetic resonance imaging (MRI) show that diffusional fractional anisotropy (FA) and kurtosis anisotropy (KA) of water inside brain white matter decrease for schizophrenic patients from that for healthy persons. DTI and DKI are statistical approaches and do not directly point to the underlying neurobiological reasons. In schizophrenia, it is believed that the demyelination of axons—microstructures that constitute the brain white matter—increases lateral diffusion of water and causes defective neural communications, resulting cognitive processing-speed deficits. Here, we use a simple but realistic neurobiological model for brain white matter and solve the Bloch-Torrey equation using numerical finite-element method to find out the underlying reasons of cognitive deficits in schizophrenia. FA and KA are calculated from computationally obtained diffusion-weighted MRI data after a Stejskal-Tanner gradient pulse sequence is applied to a periodic array of tubular axons with circular cross-sections. The calculated FA and KA decrease when the axon walls are more permeable to water, agree with the experimental findings, and correlate with the cognitive processing speeds of healthy persons and schizophrenic patients, and thus, help to understand the underlying reasons of cognitive processing-speed deficits in schizophrenia.

Introduction

Cognitive processes depend on the fast and efficient information transmission between different areas in brain. The information transmission for cognitive processes occurs mainly through the corpus callosum, which consists of millions of white matter fiber tracts and connects different areas in brain [1]. Therefore, the cognitive processing speed depends on the integrity of brain white matter [2, 3], and may suffer loss if communications between different areas in brain are defective due to disintegrated white matter [4]. The deficit in cognitive processing speed is identified as an inherent and key debilitating cognitive feature associated with schizophrenia [5–7]. Therefore, cognitive deficits may also be seen in an attenuated form in non-ill first-degree relatives of schizophrenic patients [8, 9].

The neurobiological abnormalities associated with schizophrenia are usually small and subtle, and therefore, difficult to identify by post-mortem investigation [4]. Magnetic resonance imaging (MRI) is often helpful to visualize biological structures inside human body including different areas of brain [10]. Particularly, diffusion-weighted MRI with the Stejskal-Tanner gradient pulse sequence probes diffusion of water molecules in a three-dimensional space, and hence, can provide information about microscopic tissue structures [11]. Statistical models—diffusion tensor imaging (DTI) and diffusion kurtosis imaging (DKI)—are used to analyze diffusion-weighted MRI data obtained from brain white matter to identify the underlying neurobiological reasons of schizophrenia [12, 13]. DTI studies show that the diffusion of water is anisotropic inside the white matter of a healthy brain, while the anisotropy decreases significantly inside that of a schizophrenic brain suffering from cognitive deficits [3, 14–16]. DKI statistically fits the diffusion-weighted MRI data with a higher-order model than DTI when the gradient pulse sequence is strong—the so-called b-parameter $\gg 1000$ s mm^{-2}—so that the diffusion characteristics can no longer be approximated as Gaussian [17, 18]. Diffusional fractional anisotropy (FA) and kurtosis anisotropy (KA)

calculated from DKI can provide an improved measure for the microscopic cellular structures [17, 19]. Recently, DKI analysis of diffusion-weighted MRI data obtained from corpus callosum of brain has shown that there are significant differences in FA and KA values between healthy controls, schizophrenic patients, and non-ill siblings of schizophrenic patients, and the differences in anisotropies are correlated with the differences in the cognitive processing speeds measured by digit symbol substitution test (DSST) from the same sample groups [20].

The differences in the mean diffusional anisotropies between healthy controls, schizophrenic patients, and non-ill siblings of schizophrenic patients obtained from DTI and DKI analyses have been linked to the different levels of the integrity of white matter in corpus callosum [20–23]. Although the statistical approaches link the loss of cognitive processing speed to the lack of integrity of the white matter, i.e., when the myelin sheath around the axons fails to sufficiently restrict the water diffusion in the lateral direction, the diffusion-weighted MRI findings do not categorically point to the underlying biological reasons. However, a theoretical analysis considering a realistic biological structure of corpus callosum that can relate the differences in FA and KA findings from healthy controls, schizophrenic patients, and non-ill siblings of schizophrenic patients to the different levels of the integrity of white matter is lacking but would be immensely helpful to understand the impact of neurobiology on the cognitive processing speed.

The diffusion-weighted MRI data, and hence, the FA and KA using DTI and DKI approaches can be calculated by solving the Bloch-Torrey equation (BTE) [24, 25]. However, BTE cannot be solved analytically in realistic geometries without additional assumptions. Sukstanskii *et al.* used a simplified one-dimensional model of brain white matter to solve BTE to understand the restricted diffusion at the axon boundaries [26, 27]. While a one-dimensional model shows importance of restricted diffusion, it is physically apparent that the simplest geometry that can reproduce the expected diffusion of water in and around axons must be two-dimensional. There has been significant work done on biophysical modeling of diffusion-weighted MRI of brain white matter [28]. Biophysical models are effectively empirical models, based on the assumption that the white matter is composed of different compartments that have different diffusion coefficients associated with both the longitudinal and transverse directions of flow relative to the axons. These models vary widely in terms of the number of free parameters, and the parameters must fit to the data.

Computational work to obtain exact solutions of the BTE for realistic neurobiological geometries in the brain appears to be in its infancy. Finite-difference method (FDM) has been used to solve BTE to study the diffusion-weighted MRI data [29–31]. However, square-grid-based FDM exaggerates the size and shape of microscopic axons. Limited studies have also been reported based on finite-element method (FEM) [32]. However, no computational work has attempted to apply these models to analysis of DTI or DKI experiments. We believe that the development of physics-based models that solve the BTE exactly within the limits of computational accuracy have the potential to transform our understanding of the microscopic processes that underlie the observations in DTI or DKI experiments.

In this work, we use FEM to solve BTE for a simple but realistic geometry of white matter. The neurobiological model parameters are based on their actual values observed in post-mortem studies except the permeability of the myelin sheath. The integrity of the white matter for healthy controls, schizophrenic patients, and non-ill siblings of schizophrenic patients is included in the model by the variation of the permeability of the myelin sheath. We find that the results obtained using this heuristic approach agree with the experimental observations, and correlate well with the cognitive processing speeds of healthy controls, schizophrenic patients, and non-ill siblings of schizophrenic patients obtained from DSST.

Physical model for brain white matter

Corpus callosum—the largest white matter structure in the human brain—consists of 200–250 million slender, long axons that conduct electrical impulses between the left and right hemispheres of a human brain [33]. For efficient conduction of electrical impulses, axons are surrounded by an insulating layer of myelin—a fatty white substance. Myelin sheath obstructs the diffusion of water molecules in the lateral direction and increases the electrical resistance across the boundary of the axons so that the saltatory conduction of electrical impulses inside the myelinated axons can be fast and efficient [34]. Therefore, in the white matter of a healthy brain, water molecules diffuse at a much faster rate in the longitudinal direction of axons than in the transverse direction. However, post-mortem studies show evidences of disintegration in brain white matter and diffusion-weighted MRI studies performed on brain white matter show a decrease in FA and KA for schizophrenic patients. The post-mortem and diffusion-weighted MRI observations about a schizophrenic patient are usually linked to the demyelination of axons [20–23].

Axon diameters vary over a range of 0.2–10 μm in the three distinct regions of corpus callosum: Genu, body, and splenium [35]. While large diameter axons are more common in mid- and posterior-body regions of corpus callosum, ~72% of axons in genu have a diameter <1 μm [35]. Among different regions of corpus callosum, genu is principally responsible for cognitive processing. The large diameter axons in other areas of

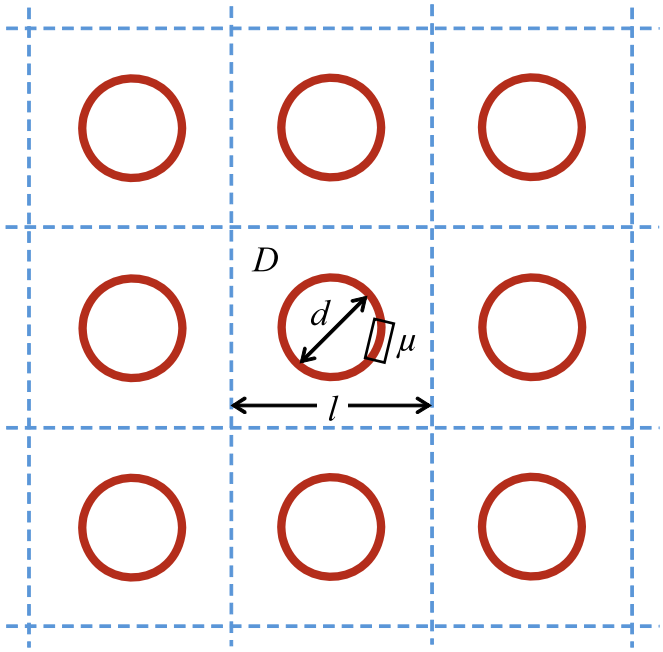

Figure 1. Cross-sectional view of corpus callosum model used in this work with periodic tubular circular axons.

corpus callosum are usually responsible for visual and somatosensory processes [36, 37]. Post-mortem studies show an average axon diameter of ∼0.6 μm in genu [35]. However, the estimated axon diameters in post-mortem studies are less than actual due to the shrinkage in the processing involved in measurement. The axon diameters are found to shrink to ∼65% of their actual sizes, so that a measured 0.6 μm diameter axon actually corresponds to an axon with ∼1 μm diameter *in vivo* [35]. Axons have an average density of $\sim 3.717 \times 10^5$ axons/mm^2 in genu [35], which corresponds to one axon in every ∼2.7 μm^2. Therefore, when the shrinkage factor is taken into consideration, axons have an average separation or periodicity of ∼2.5 μm.

To model the water diffusion inside corpus callosum in diffusion-weighted MRI with the Stejskal-Tanner gradient pulse sequence, we consider a periodic array of tubular axons with circular cross-sections. Figure 1 shows a cross-sectional view of a 3×3 array of axons in the transverse plane. The dimension of axons in the longitudinal direction is much greater than the diffusion length of water so that the diffusion in the longitudinal direction can be considered unrestricted. The diffusion coefficient of water is same for both inside and outside the axons. However, the diffusion of water through the axon boundary is restricted and is different for healthy controls and schizophrenic patients depending on the integrity of the myelin sheath. The structure, as shown in figure 1, is characterized by four parameters d, l, μ, and D, where d is the diameter of axons, l is the separation between axons, μ is the permeability of myelin sheath around axons, and D is the free diffusion coefficient of water molecules.

In this work, we assume a fixed periodicity $l = 2.5$ μm and diffusion coefficient $D = 1$ μm^2/ms for both intra- and extra-axonal media. We treat d as a random variable with a probability density function (PDF). We study the changes in anisotropies with μ for both Gaussian and Gamma PDFs for d. While a Gaussian PDF for d will let us easily follow the changes in anisotropies with μ as d varies for a better understanding, a Gamma PDF for d will approximate the actual distribution of d better [38]. We note that treating d as a random variable corresponds physically to allow a gradual variation in the axon diameter over the very large dimensions of a voxel probed in diffusion-weighted MRI and also in different persons. We also consider μ as a random variable. We find out μ values heuristically for healthy controls, schizophrenic patients, and non-ill siblings of schizophrenic patients so that the calculated FA and KA agree with those obtained in experiments and can be correlated with the processing speeds of healthy controls, schizophrenic patients, and non-ill siblings of schizophrenic patients obtained in DSST. While simple, we will show that this model is sufficiently complex to account for the anisotropies observed in DKI experiments.

Theoretical model

In diffusion-weighted MRI, the evolution and dynamics of magnetization of water molecules during excitation and relaxation are described by the phenomenal Bloch-Torrey equation (BTE) given by [24, 25]

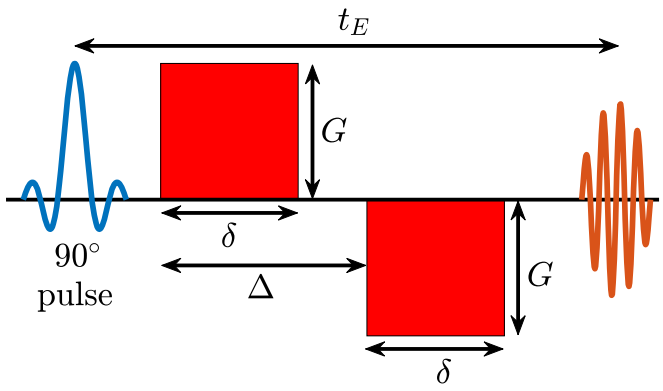

Figure 2. Stejskal-Tanner gradient pulse sequence.

$$\frac{\partial \mathbf{M}}{\partial t} = \gamma \mathbf{M} \times \mathbf{B} - \begin{pmatrix} \frac{1}{T_2} & 0 & 0 \\ 0 & \frac{1}{T_2} & 0 \\ 0 & 0 & \frac{1}{T_1} \end{pmatrix} \mathbf{M} + \begin{pmatrix} 0 \\ 0 \\ \frac{M_0}{T_1} \end{pmatrix} - \nabla \cdot D\nabla \mathbf{M}, \tag{1}$$

where **M** is the local magnetization, M_0 is the equilibrium magnetization, **B** is the applied magnetic field, T_1 is the spin-lattice or longitudinal relaxation time, T_2 is the spin-spin or transverse relaxation time, γ is the gyromagnetic constant for the medium, and D is the diffusion coefficient of the medium. The term $\nabla \cdot D\nabla\mathbf{M}$ reduces to $D\nabla^2\mathbf{M}$ when D is a constant. BTE has led to the development of various pulse sequences, which allow us to calculate the diffusivity of water molecules in a complex microscopic scale geometry from diffusion-weighted signals, and hence, develop a diffusion-weighted MRI image [11, 39].

In MRI, a spin-echo is created after a 90° pulse is applied to a pool of water molecules precessing around a fixed magnetic field in the z-direction. In diffusion-weighted MRI, spin-echo signal is measured after a gradient pulse sequence is applied so that water molecules diffuse in the direction of the gradient. If a z-directional gradient field **g** that varies linearly in the transverse direction is superposed on a z-directional uniform magnetic field B_0, then the total applied magnetic field at a position **r** is $B = B_0 + \mathbf{g} \cdot \mathbf{r}$. Now, neglecting the relaxation due to T_1 and assuming that the complex transverse magnetization is a vector in the complex x-y plane, which precesses about the z-axis with an angular velocity ω_0, we can write [24]

$$\frac{\partial S}{\partial t} = -i\gamma \mathbf{g} \cdot \mathbf{r} S + D\nabla^2 S, \tag{2}$$

where S represents the amplitude of the precessing magnetization that is not affected by spin-spin relaxation, so that $M_x + iM_y = S\exp[-(i\omega_0 + 1/T_2)t]$. In diffusion-weighted MRI, we are interested in calculating the spin-echo signal

$$s(t) = \int_A S(\mathbf{r}, t)\, dA, \tag{3}$$

where the integration is over the area of one voxel.

In figure 2, we show a schematic illustration of the Stejskal-Tanner gradient pulse sequence that we used in this work. The gradient pulse sequence is described by three parameters—the amplitude of the gradient pulses G, the duration of the gradient pulses δ, and the duration between the starts of the gradient pulses Δ. The echo signal is calculated at time t_E. The strength of the gradient pulse sequence is often described by a diffusion-sensitizing gradient coefficient $b = (\gamma\delta G)^2(\Delta - \delta/3)$. In this work, we assume $\delta = 47$ ms, $\Delta = 54$ ms, and $t_E = 120$ ms for the gradient pulse sequence, similar to that used in [20]. We have varied b from zero to 2500 s mm^{-2} at an interval of 250 s mm^{-2}.

We solve BTE using FEM on COMSOL Multiphysics platform. We select physics-controlled mesh so that COMSOL Multiphysics creates a mesh that is adapted to the physics interface settings and the geometry of the model. We choose extra fine element sizes. In figure 3, we show mesh elements that are used to solve BTE when the axon diameter is 0.8 and 1.6 μm. We solve only a two-dimensional structure as the structure can be assumed invariant in the other direction as the water diffusion is not restricted in the vertical z-direction.

Results

In this work, we apply Stejskal-Tanner gradient pulse sequences in the transverse and longitudinal directions of a periodic fiber bundle as shown in figure 1, and calculate the diffusion-weighted echo signals in the

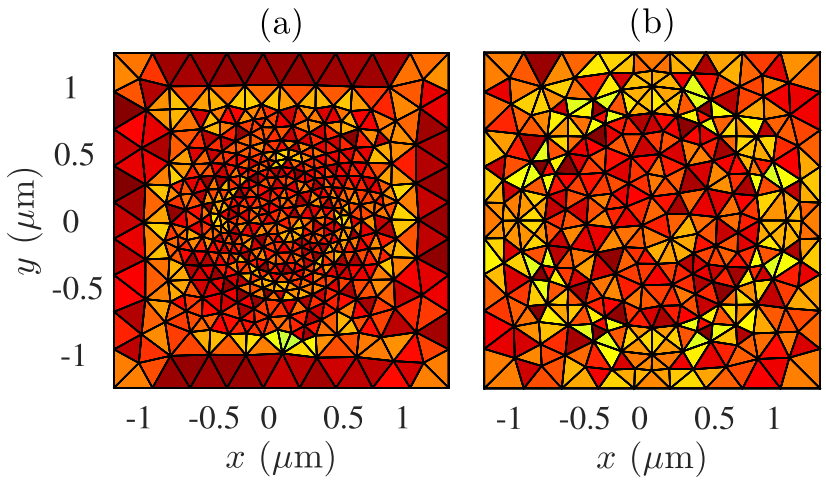

Figure 3. Finite-element mesh grids for one period of the periodic array of axons when the axon diameter is (a) 0.8 μm and (b) 1.6 μm. The colors are used merely to show the finite-element mesh grids distinct.

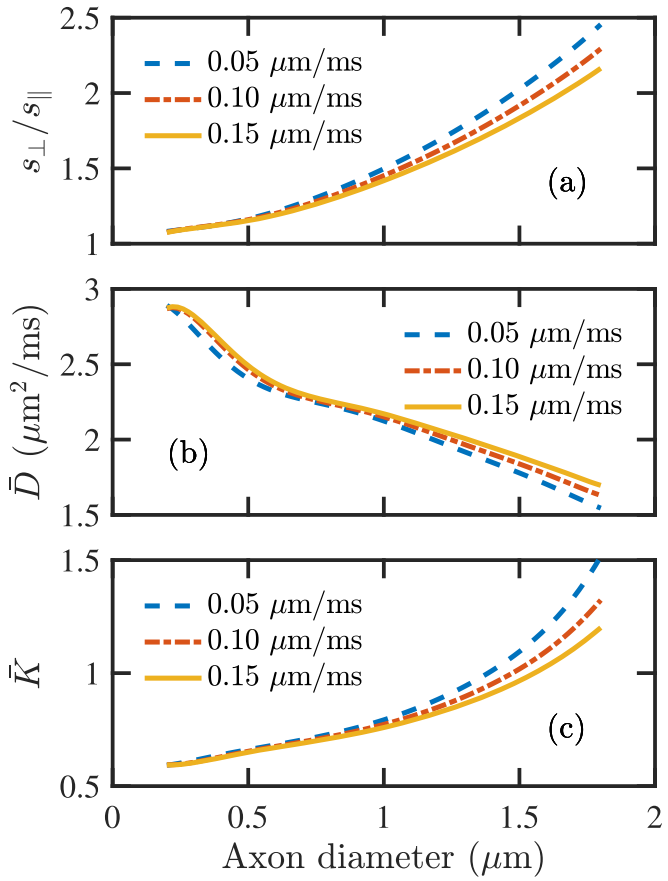

Figure 4. (a) Ratio of diffusion-weighted signal in the transverse plane to that in the longitudinal plane ($s_\perp/s_\parallel$) versus the diameter of axons for different permeabilities of myelin sheath. The gradient pulse sequence is applied with $b = 1500$ s mm^{-2}. Mean (b) diffusion ($\bar{D}$) and (c) kurtosis ($\bar{K}$) coefficients at $b = 1500$ s mm^{-2}.

transverse ($s_\perp$) and longitudinal planes ($s_\parallel$) at time t_E. We vary the diffusion-sensitizing gradient coefficient b and axon diameter d. We use $s_\perp$ and $s_\parallel$ to calculate the radial ($D_\perp$), axial ($D_\parallel$), and mean ($\bar{D}$) diffusion coefficients for varying d. We also calculate the radial ($K_\perp$), axial ($K_\parallel$), and mean ($\bar{K}$) kurtosis coefficients. Then we use the radial, axial, and mean diffusion and kurtosis coefficients to calculate the diffusional FA and KA using the approach described in the Method section.

In figure 4, we show the ratio of diffusion-weighted signal in the transverse plane to that in the longitudinal plane ($s_\perp/s_\parallel$), $\bar{D}$, and $\bar{K}$ as d varies. We note that $s_\perp/s_\parallel$ presented in figure 4(a) is obtained when

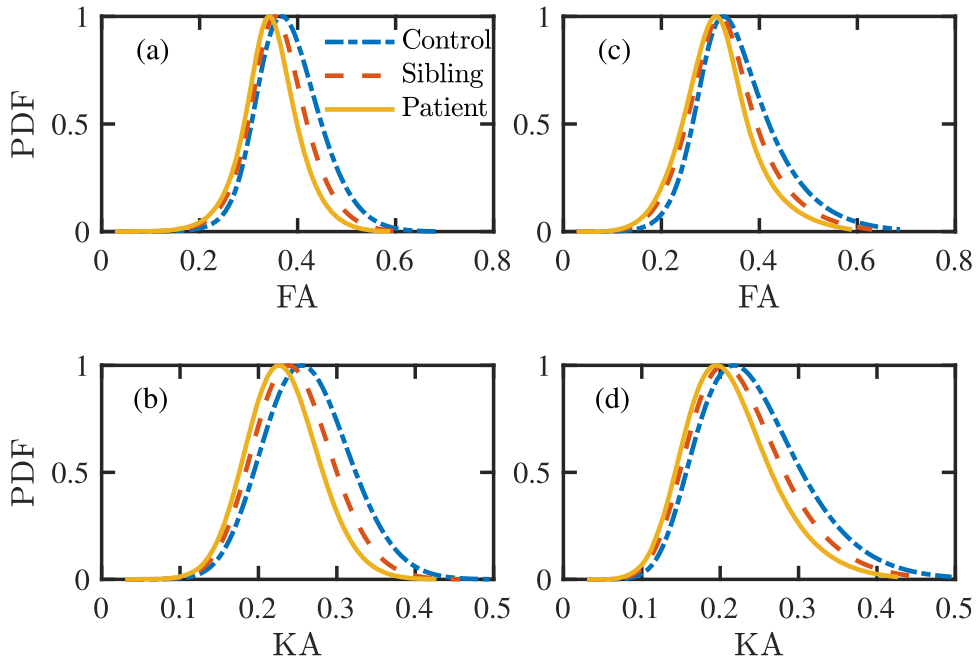

Figure 5. Normalized PDF of (a) FA and (b) KA with Gaussian PDF for d, and (c) FA and (d) KA with Gamma PDF for d for healthy controls, siblings, and patients obtained from finite-element simulations. We assume that $\mu = 0.05, 0.10$, and 0.15 μm/ms represent healthy controls, non-ill siblings of schizophrenic patients, and schizophrenic patients, respectively. The legends in (a) apply for (b)–(d) as well.

$b = 1500$ s mm^{-2}, and $\bar{D}$ and $\bar{K}$ presented in figures 4(b) and 4(c) are calculated using $s_\perp$ and $s_\parallel$ values obtained at $b = 1000$, 1250, and 1500 s mm^{-2}. Here, we assume the permeability of the myelin sheath $\mu = 0.05$, 0.10, and 0.15 μm/ms. We calculated the diffusion-weighted signals and the diffusion coefficients over a broad range of μ including when the myelin sheath is completely restricting, i.e., $\mu = 0$. However, we present the results when $\mu = 0.05, 0.10$, and 0.15 μm/ms since assuming these realistic permeability values for healthy controls, non-ill siblings of schizophrenic patients, and schizophrenic patients, respectively, fits the calculated FA and KA well with the FA and KA values measured in human subjects in-vivo [20]. In figure 4, we note that $s_\perp/s_\parallel > 1$, and $s_\perp/s_\parallel$ increases as d increases and μ decreases. In the transverse plane, the diffusion of magnetized water molecules is restricted by the limited permeability of the myelin sheath, while they are relatively free in the longitudinal direction. Therefore, the diffusion-weighted signal decays more in the longitudinal direction than in the transverse direction due to diffusion of water molecules in the presence of a gradient pulse sequence. Also, the amount of restricted water molecules increases as d increases. Therefore, $s_\perp/s_\parallel$ also increases as d increases. The restricted diffusion in the transverse plane causes $\bar{D}$ to decrease as d increases. However, as the water molecules are more restricted when μ decreases or d increases, the diffusion characteristics deviate more from a Gaussian distribution. Therefore, we note that $\bar{K}$ increases when μ decreases or d increases. We found that with a non-permeable myelin sheath, i.e., $\mu = 0$, although the parameters $s_\perp/s_\parallel$, $\bar{D}$, and $\bar{K}$ do not vary much compared to a permeable membrane, i.e., $\mu > 0$, when $d \lesssim 0.5$ μm, the parameters significantly vary when d increases. In particular, we found $s_\perp/s_\parallel \approx 3$, $\bar{D} \approx 1.38$ μm^2/ms, and $\bar{K} \approx 3$ with $\mu \approx 0$ when $d = 1.8$ μm. We note that the results presented in figure 4 qualitatively match with that presented in [28] calculated using biophysical models.

In figure 5, we show the normalized PDFs for FA and KA for healthy controls, non-ill siblings of schizophrenic patients, and schizophrenic patients obtained from finite-element simulations, where we have assumed $\mu = 0.05$, 0.10, and 0.15 μm/ms represent healthy controls, non-ill siblings of schizophrenic patients, and schizophrenic patients, respectively. We assume two cases: In one case, d has a Gaussian PDF, and in the other case, d has a Gamma PDF. In both cases, we note that the peak positions of PDFs for both FA and KA have higher values for healthy controls than that for schizophrenic patients or non-ill siblings of schizophrenic patients. Overall, the PDFs for both FA and KA are shifted to higher anisotropies and become non-Gaussian or skewed toward higher values more for healthy controls than for schizophrenic patients or non-ill siblings of schizophrenic patients. Similarly, the PDFs for both FA and KA are shifted to higher anisotropies and become non-Gaussian more for non-ill siblings of schizophrenic patients than for schizophrenic patients.

In figure 6, we show the mean and standard deviation of FA and KA for healthy controls, non-ill siblings

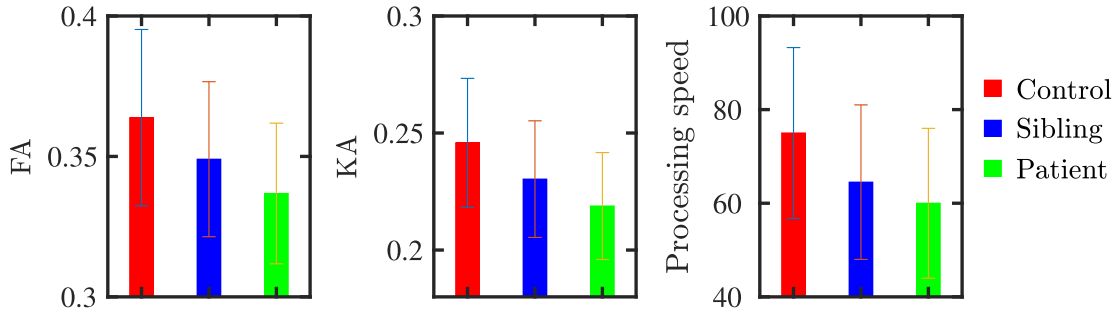

Figure 6. Mean and standard deviation of FA, KA, and cognitive processing speed for healthy controls, siblings, and patients. Mean and standard deviation of FA and KA are obtained from finite-element simulations assuming that $\mu = 0.05, 0.10$, and 0.15 μm/ms represent healthy controls, non-ill siblings of schizophrenic patients, and schizophrenic patients, respectively, and a Gaussian PDF for d. Processing-speed data are taken from [20].

of schizophrenic patients, and schizophrenic patients obtained from finite-element simulations, where we have assumed $\mu = 0.05, 0.10$, and 0.15 μm/ms represent healthy controls, non-ill siblings of schizophrenic patients, and schizophrenic patients, respectively. We also show the mean and standard deviation of cognitive processing speeds of healthy controls, non-ill siblings of schizophrenic patients, and schizophrenic patients measured using DSST and reported in [20]. We note that the calculated FA and KA assuming that $\mu = 0.05$, 0.10, and 0.15 μm/ms represent healthy controls, non-ill siblings of schizophrenic patients, and schizophrenic patients, respectively, are correlated with the cognitive processing speeds of healthy controls, non-ill siblings of schizophrenic patients, and schizophrenic patients, respectively, measured using DSST.

Discussion

This work shows that the DKI findings about the changes in anisotropies for water diffusion and the correlated cognitive processing speeds can be linked to the underlying neurobiology as the change in the permeability of the myelin sheath around a periodic array of tubular circular axons. The FEM-based solutions of BTE and the heuristic approach for the permeability of the myelin sheath show that FA and KA are greater for intact axons in brain white matter, whereas FA and KA are smaller for disintegrated axons. A healthy person with intact axons in brain white matter has less water diffusion in the lateral direction through the myelin sheath than that of a patient suffering from cognitive deficits and non-ill siblings of schizophrenic patients with disintegrated axons in the brain white matter. Therefore, the mean FA and KA of healthy persons are greater than that for schizophrenic patients and non-ill siblings of schizophrenic patients. Although the PDF of the axon diameter has been assumed Gaussian, the calculated PDFs of FA and KA with the distribution of axon diameter are non-Gaussian. The non-Gaussian behavior of PDFs of FA and KA is stronger in healthy controls than in schizophrenic patients or non-ill siblings of schizophrenic patients.

We find that the mean anisotropies are relatively smaller than that found in [20]. This discrepancy is attributed to the fact that the PDF of axon diameter is not Gaussian rather skewed to larger diameter values and the DKI experiments of [20] probed voxels from outside genu, which have axons with larger diameters. Since the anisotropies increase with the increase of axon diameter, a non-Gaussian PDF of axon diameter biased with larger values and voxels with axons of larger diameter will increase the mean values of anisotropies. Also, the increase in anisotropy will be greater for healthy controls than that for patients or siblings of patients. The discrepancy can also be attributed partly to the orientation dispersion of the axons due to their non-parallel alignment in contrast to the parallel orientation considered in this work. Additionally, in reality, the axons will not be periodically packed, rather the inter-axonal displacements will vary within a voxel. The irregular inter-axonal displacements may also contribute to the changes observed in FA and KA in schizophrenia. A more complex theoretical model that includes the irregular axonal orientation and displacement parameters may relate the underlying neurobiology more closely with the diffusion weighted MRI findings, and hence, also with the processing speed deficit in schizophrenia.

Methods

The FEM-based solution of BTE gives us the diffusion-weighted signal s, which is a function of the gradient pulse sequence. The diffusion-weighted signal s at a particular value of b can be given by using the Taylor series [18, 40, 41]

$$\ln[s(b)] = \ln(s_0) - bD + \frac{1}{6}b^2D^2K + O(b^3), \quad (4)$$

where D is the apparent diffusion coefficient, K is the apparent diffusional kurtosis, and s_0 is the diffusion-weighted signal at $b = 0$. In equation (4), $O(b^3)$ terms

can be neglected for $b \lesssim 3000$ s/mm^2 and an equation for $s(b)$ can be written as

$$\ln[s(b)] \approx \ln(s_0) - bD + \frac{1}{6}b^2D^2K. \quad (5)$$

Equation (5) can be used for DKI analysis, and the radial, axial, and mean diffusion and kurtosis coefficients can be calculated if diffusion-weighted signals in the radial and axial directions are known for three b values. If diffusion-weighted signals are known for $b = b_1$, b_2, and b_3, D and K can be calculated in the direction of the applied gradient field as [42]

$$D \approx \frac{(b_3 + b_1)D^{(12)} - (b_2 + b_1)D^{(13)}}{b_3 - b_2}, \quad (6)$$

and

$$K \approx 6\,\frac{D^{(12)} - D^{(13)}}{(b_3 - b_2)D^2}, \quad (7)$$

where

$$D^{(12)} = \frac{\ln[s(b_1)/s(b_2)]}{b_2 - b_1}, \quad D^{(13)} = \frac{\ln[s(b_1)/s(b_3)]}{b_3 - b_1}. \quad (8)$$

Now, FA can be calculated as

$$\mathrm{FA} = \sqrt{\frac{3}{2}\frac{(\lambda_1 - \bar{D})^2 + (\lambda_2 - \bar{D})^2 + (\lambda_3 - \bar{D})^2}{\lambda_1^2 + \lambda_2^2 + \lambda_3^2}}, \quad (9)$$

where λ_1, λ_2, and λ_3 are the eigenvalues of a diffusion tensor matrix in the three principal axes, and are related to $D_{\|}$, $D_{\perp}$, and $\bar{D}$ as $D_{\|} = \lambda_1$, $D_{\perp} = (\lambda_1 + \lambda_2)/2$, and $\bar{D} = (\lambda_1 + \lambda_2 + \lambda_3)/3$. KA can be calculated in a similar way given by [17]

$$\mathrm{KA} = \sqrt{\frac{3}{2}\frac{(K_1 - \bar{K})^2 + (K_2 - \bar{K})^2 + (K_3 - \bar{K})^2}{K_1^2 + K_2^2 + K_3^2}}, \quad (10)$$

where K_1, K_2, and K_3 are the eigenvalues of kurtosis tensor matrix in the three principal axes, and are related to $K_{\|}$, $K_{\perp}$, and $\bar{K}$ as $K_{\|} = K_1$, $K_{\perp} = (K_1 + K_2)/2$, and $\bar{K} = (K_1 + K_2 + K_3)/3$.

To calculate the mean and standard deviation of FA and KA due to varying μ at the axon boundary, we assume that d has a Gaussian or Gamma PDF. Although d in genu of corpus callosum can be approximated by an average value of $\sim 1\,\mu$m, the actual values may vary over a relatively broad range from $\sim 0.2\,\mu$m to $\gtrsim 2\,\mu$m [35]. Strictly speaking, the PDFs of axons may not be Gaussian, rather skewed to the larger diameter values. PDFs of FA and KA are calculated by multiplying the calculated FA and KA for varying d by the Gaussian or Gamma PDF of d.

Acknowledgments

The author gratefully acknowledges the discussions with Curtis R. Menyuk and Peter Kochunov in identifying the scientific problem approached in this work. The author also acknowledges helpful suggestions from Curtis R. Menyuk and Peter Kochunov in the preparation of this manuscript.

ORCID iDs

Muhammad Anisuzzaman Talukder https://orcid.org/0000-0002-2814-3658

References

[1] Gruzelier J H 1991 *Handbook of Schizophrenia: Neuropsychology, Psycho-physiology and Information Processing* vol. 5 (New York, NY: Elsevier) 599–650 ch. Hemispheric imbalance: syndromes of schizophrenia, premorbid personality, and neurodevelopmental influences

[2] Madden D J, Bennett I J and Song A W 2009 Cerebral white matter integrity and cognitive aging: Contributions from diffusion tensor imaging *Neuropsychology Review*. **19** 415–35

[3] Penke L *et al* 2010 A general factor of brain white matter integrity predicts information processing speed in healthy older people *The Journal of Neuroscience* **30** 7569–74

[4] Shenton M E, Dickey C C, Frumin M and McCarley R W 2001 A review of mri findings in schizophrenia *Schizophrenia Research* **49** 1–52

[5] Nuechterlein K H *et al* 2004 Identification of separable cognitive factors in schizophrenia *Schizophrenia Research* **72** 29–39

[6] Fioravanti M, Carlone O, Vitale B, Cinti M E and Clare L 2005 A meta-analysis of cognitive deficits in adults with a diagnosis of schizophrenia *Neuropsychology Review* **15** 73–95

[7] Green M F 2006 Cognitive impairment and functional outcome in schizophrenia and bipolar disorder *The Journal of Clinical Psychiatry* **67** e12

[8] Finkelstein J R, Cannon T D J, Gur R E, Gur R C and Moberg P 1997 Attentional dysfunctions in neuroleptic-naive and neuroleptic-withdrawn schizophrenic patients and their siblings *Journal of Abnormal Psychology* **106** 203–12

[9] Gold J M 2004 Cognitive deficits as treatment targets in schizophrenia *Schizophrenia Research* **72** 21–8

[10] McRobbie D W, Moore E A, Graves M J and Prince M R 2006 *MRI From Picture to Proton* 2nd Edn. (Cambridge, UK: Cambridge University Press)

[11] Stejskal E O and Tanner J E 1965 Spin diffusion measurement: Spin echoes in the presence of a time-dependent field gradient *J. Chem. Phys.* **42** 288–92

[12] Basser P J, Mattiello J and LeBihan D 1994 Estimation of the effective self-diffusion tensor from the nmr spin echo *Journal of Magnetic Resonance, Series B* **103** 247–54

[13] Mori S and Zhang J 2006 Principles of diffusion tensor imaging and its applications to basic neuroscience research *Neuron* **51** 527–39

[14] Wright S N *et al* 2015 Perfusion shift from white to gray matter may account for processing speed deficits in schizophrenia *Human Brain Mapping* **36** 3793–804

[15] Nazeri A *et al* 2013 Alterations of superficial white matter in schizophrenia and relationship to cognitive performance *Neurophychopharmacology* **38** 1954–62

[16] Ellison-Wright I and Bullmore E 2009 Meta-analysis of diffusion tensor imaging studies in schizophrenia *Schizophrenia Research* **108** 3–10

[17] Hui E S, Cheung M M, Qi L and Wu E X 2008 Towards better mr characterization of neural tissues using directional diffusion kurtosis analysis *Neuroimage* **42** 122–34

[18] Jensen J H, Helpern J A, Ramani A, Lu H and Kaczynski K 2005 Diffusional kurtosis imaging: The quantification of non-gaussian water diffusion by means of magnetic resonance imaging *Magn. Reson. Med.* **53** 1432–40

[19] Glenn G R, Helpern J A, Tabesh A and Jensen J H 2015 Quantitative assessment of diffusional kurtosis anisotropy *NMR Biomed.* **28** 448–59
[20] Kochunov P *et al* 2016 Diffusion-weighted imaging uncovers likely sources of processing-speed deficits in schizophrenia *Proc. Natl Acad. Sci.* **113** 13504–9
[21] Tkachev D *et al* 2003 Oligodendrocyte dysfunction in schizophrenia and bipolar disorder *The Lancet* **362** 798–805
[22] Uranova N *et al* 2001 Electron microscopy of oligodendroglia in severe mental illness *Brain Res. Bull.* **55** 597–610
[23] Uranova N A, Vikhreva O V, Rachmanova V I and Orlovskaya D D 2011 Ultrastructural alterations of myelinated fibers and oligodendrocytes in the prefrontal cortex in schizophrenia: A postmortem morphometric study *Schizophrenia Research and Treatment* 325789
[24] Torrey H C 1956 Bloch equations with diffusion terms *Phys. Rev.* **104** 563
[25] Minati L and Weglarz W P 2007 Physical foundations, models, and methods of diffusion magnetic resonance imaging of the brain: A review *Concepts in Magnetic Resonance Part* A **30A** 278–307
[26] Sukstanskii A L and Yablonskiy D A 2002 Effects of restricted diffusion on mr signal formation *J. Magn. Reson.* **157** 92–105
[27] Sukstanskii A L, Ackerman J J H and Yablonskiy D A 2003 Effects of barrier-induced nuclear spin magnetization inhomogeneities on diffusion-attenuated mr signal *Mangnetic Resonance in Medicine* **50** 735–42
[28] Nilsson M, van Westen D, Støahlberg F, Sundgren P C and Lätt J 2013 The role of tissue microstructure and water exchange in biophysical modelling of diffusion in white matter *Magn. Reson. Mater. Phys., Biol. Med.* **26** 345–70
[29] Hwang S N, Chin C-L, Wehrli F W and Hackney D B 2003 An image-based finite difference model for simulating restricted diffusion *Magn. Reson. Med.* **50** 373–82
[30] Xu J, Does M D and Gore J C 2007 Numerical study of water diffusion in biological tissues using an improved finite difference method *Phys. Med. Biol.* **52** N111–26
[31] Russell G, Harkins K D, Secomb T W, Galons J P and Trouard T P 2012 A finite-difference method with periodic boundary conditions for simulations of diffusion-weighted magnetic resonance experiments in tissue *Phys. Med. Biol.* **57** N35–46
[32] Nguyen D V, Li J-R, Grebenkov D and Bihan D L 2014 A finite element method to solve the bloch-torrey equation applied to diffusion magnetic resonane imaging *J. Comput. Phys.* **263** 283–302
[33] Ludres E, Thompson P M and Toga A W 2010 The development of the corpus callosum in the healthy human brain *J. Neurosci.* **30** 10985–90
[34] Hildebrand C, Remahl S, Persson H and Bjartmar C 1993 Myelinated nerve fibres in the cns *Prog. Neurobiol.* **40** 319–84
[35] Aboitiz F, Scheibel A B, Fisher R S and Zaidel E 1992 Fiber composition of the human corpus callosum *Brain Res.* **598** 143–53
[36] Aboitiz F, Zaidel E and Scheibel A B 1989 Variability in fiber composition in different regions of the corpus callosum in humans *Anat. Rec.* **223** 6A
[37] Lamantia A-S and Rakic P 1990 Cytological and quantitative characteristics of four cerebral commissures in the rhesus monkey *The Journal of Comparative Neurology* **291** 520–37
[38] Assaf Y, Blumenfeld-Katzir T, Yovel Y and Basser P J 2008 Axcaliber: A methodfor measuring axon diameter distribution from diffusion mri *Magn. Reson. Med.* **59** 1347–54
[39] Carr H Y and Purcell E M 1954 Effects of diffusion on free precession in nuclear magnetic resonance experiments *Phys. Rev.* **94** 630
[40] Tanner J E 1978 Transient diffusion in a system partitioned by permeable barriers. application to nmr measurements with a pulsed field gradient *J. Chem. Phys.* **69** 1748–54
[41] Liu C, Bammer R, Acar B and Moseley M E 2004 Characterizing non-gaussian diffusion by using generalized diffusion tensors *Magn. Reson. Med.* **51** 924–37
[42] Jensen J H and Helpern J A 2010 Mri quantification of non-gaussian water diffusion by kurtosis analysis *NMR Biomed.* **23** 698–710